Disturbance Observer-Based Hysteresis Compensation for Piezoelectric Actuators

Steven Chang, Jingang Yi, and Yantao Shen

Abstract— We present a novel hysteresis compensation method for piezoelectric actuators. Instead of using any particular mathematical model of hysteresis, we consider the hysteresis nonlinearity as a disturbance over a linear system. A disturbance observer (DOB) is then utilized to estimate and compensate for the hysteresis nonlinearity. In contrast to the existing inverse model-based approaches, the DOB-based hysteresis compensation does not rely on any particular hysteresis model, and therefore provides a simple and effective compensation mechanism. Experimental validation of the proposed hysteresis compensation is performed on a PMN-PT cantilever piezoelectric actuator.

I. INTRODUCTION

During the last decade, micro-/nano-manipulation have been extensively studied in robotics and control communities [1], [2]. For manipulation platforms, for example, atomic force microscope (AFM), piezoelectric cantilever beams and piezoelectric tubes are the most widely used actuation mechanisms. However, one of the potential issues of using these actuators is deteriorating performance and limited bandwidth due to the nonlinear hysteresis effect of the piezoelectric materials [3].

To compensate for hysteresis nonlinearity, various control strategies have been proposed in the past decade. A recent review of the hysteresis compensation methods for micro-/nano-applications can be found in [3], [4]. Among these strategies, two control structures are often used for hysteresis compensation [5]: (1) inverse-model feed forward hysteresis compensation, and (2) closed-loop feedback hysteresis compensation. The inverse-model feed forward hysteresis compensation mechanism uses an inverse hysteresis model in the feed forward loop to cancel the hysteresis nonlinearity. While this implementation does not require displacement or force sensors, an accurate mathematical model for hysteresis is essential to such an approach. Additionally, the hysteresis model is typically complicated [6], [7], and the method is prone to robustness issues due to disturbances. On the other hand, although the feedback hysteresis compensation approach requires external displacement or force sensors, it provides an effective and robust means to suppress the hysteresis nonlinearity. Moreover, the feedback approach does not rely on a precise mathematical model of the hysteresis.

In this paper, we present a novel hysteresis compensation mechanism for a piezoelectric cantilever actuator that is used for micro-/nano-manipulation applications. Our approach is based on the closed-loop compensation mechanism. Instead of precisely modeling the hysteresis, we treat the hysteresis as an external disturbance adding to the linear dynamic behavior of the cantilever actuator. Then we use a disturbance observer (DOB) to estimate and compensate for the hysteresis nonlinearity. The significance of the proposed DOB-based hysteresis compensation is its simplicity in implementation and robustness due to its independence from any mathematical models of hysteresis. We also experimentally validate the proposed compensation method on a piezoelectric cantilever actuator.

Our approach is inspired by several related works [8], [9]. In [8], a DOB-based nonlinearity cancellation is proposed for a large class of single-input single-output (SISO) nonlinear systems. The output of the nonlinear SISO system is assumed as the sum of the outputs of a stable SISO linear-time-invariant system and a bounded function of time. The nonlinearity in the system could include dead-zone, backlash, and hysteresis. In [9], a linear active disturbance rejection control (LADRC) is proposed for hysteresis compensation. Hysteresis nonlinearity is considered as a disturbance and a linear observer is proposed as a disturbance estimator. However, it is not clear why the hysteresis-induced disturbance can be treated as a linear system. Moreover, no experimental validation has been presented for the proposed approach. Our work is an extension of the approach in [8]. We use a piezoelectric cantilever actuator as an example to show that hysteresis nonlinearity can be decomposed into a bounded hysteresis operator and an approximated linear dynamic system. We relax the linear disturbance estimation assumption in [9], and provide a more comprehensive treatment for the hysteresis nonlinearity. We also provide an experimental validation.

The remainder of the paper is organized as follows. We present the DOB-based hysteresis compensation design in Section II. In Section III, we discuss modeling of a piezoelectric cantilever actuator. The experimental implementation of the DOB-based hysteresis compensator is presented in Section IV before concluding the paper in Section V.

S. Chang is with the Department of Mechanical Engineering, San Diego State University, San Diego, CA 92182 USA. Email: changs@rohan.sdsu.edu.

J. Yi is with the Department of Mechanical and Aerospace Engineering, Rutgers University, Piscataway, NJ 08854 USA. Email: jgyi@rutgers.edu.

Y. Shen is with the Department of Electrical and Biomedical Engineering, University of Nevada, Reno, NV 89557 USA. Email: ytshen@unr.edu.

II. DISTURBANCE OBSERVER-BASED HYSTERESIS COMPENSATION

In this section, we first discuss the decomposition of a class of nonlinear dynamic systems with hysteresis relationship as a component of the system. Then we present a DOB-based hysteresis compensation approach.

A. Decomposition of a class of nonlinear dynamic systems with hysteresis

Here, we consider a class of nonlinear dynamic systems in which the hysteresis nonlinear relationship is one part of the dynamics. For the piezoelectric cantilever actuator that we will discuss in the next section, the applied voltage input $v(t)$ generates a charge $q(t)$ between the electrodes. This charge then produces a deformation $y(t)$ in the piezoelectric material. The left sub-figure in Fig. 1 shows such a nonlinear relationship. We denote the hysteresis relationship between the input voltage $v(t)$ and charge $q(t)$ as

$$q(t) = (\mathcal{H}(v))(t), \tag{1}$$

where $\mathcal{H}(\cdot)$ denotes the hysteresis operator. The dynamic relationship between $q(t)$ and output $y(t)$ is given by the linear time-invariant system $P(s)$.
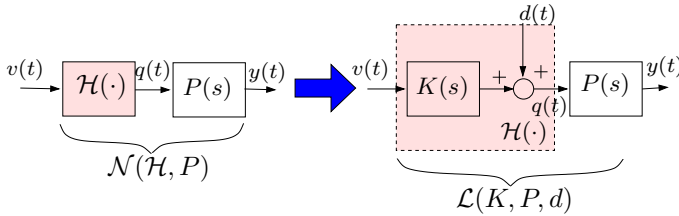

Fig. 1. Schematic of decomposition of a nonlinear system with hysteresis nonlinearity $\mathcal{H}(\cdot)$ as an integrated part of the system.

Let $\mathcal{N}(\mathcal{H}, P)$ denote the nonlinear dynamic system. We propose to decompose $\mathcal{N}(\mathcal{H}, P)$ into a linear system $\mathcal{L}(K, P, d)$ as shown in the right sub-figure in Fig. 1. Here $K(s)$ denotes a linear time-invariant relationship between input variable $v(t)$ and intermediate variable $q(t)$. Also, the disturbance $d(t)$ is a bounded nonlinear function of input $v(t)$. The intermediate variable $q(t)$, such as electric charge in piezoelectric actuators, is typically assumed unmeasurable.

To elucidate the above decomposition, we consider a Duhem model to capture the rate-independent hysteresis relationship between the input $v(t)$ and intermediate variable $q(t)$ [7], [10]. The Duhem model represents $\mathcal{H}(\cdot)$ by a first-order nonlinear differential equation as

$$\dot{q}(t) = \alpha|\dot{v}(t)|\left(av(t) - q(t)\right) + b\dot{v}(t), \tag{2}$$

where $\alpha > 0$ and $a > b \geq \frac{1}{2}a$ are model constants that depend on the shape and area of the hysteresis curves experimentally. In Eq. (2), $q(t)$ is considered as the state variable of the differential equation and depends on the values of both $v(t)$ and $\dot{v}(t)$. Such a mathematical relationship (2) can reproduce the hysteresis phenomena that we observe in

experiments. Readers can refer to [7], [10] for more details on how to estimate these hysteresis model parameters.

We consider the solution properties of the Duhem model (2). Following a similar derivation in [11], we can solve (2) explicitly as follow.

$$q(t) = \alpha v(t) + d(t), \tag{3}$$

where

$$
\begin{aligned}
d(t) &:= d(v(t)) = (q_0 - av_0)e^{-\alpha(v-v_0)\,\mathrm{sgn}(\dot{v})} \\
&\quad + e^{-\alpha v\,\mathrm{sgn}(\dot{v})}\int_{v_0}^{v}(b-a)e^{\alpha\tau\,\mathrm{sgn}(\dot{v})}d\tau, \tag{4}
\end{aligned}
$$

where $q_0 := q(0)$, $v_0 := v(0)$, and function $\mathrm{sgn}(x) = 1$ if $x \geq 0$ and $\mathrm{sgn}(x) = -1$ if $x < 0$. It is straightforward to check that for $\dot{v} > 0$ or $\dot{v} < 0$, the above solution satisfies

$$\lim_{v\to+\infty} d(t) = -\frac{a-b}{\alpha} \quad \text{or} \quad \lim_{v\to-\infty} d(t) = \frac{a-b}{\alpha} \tag{5}$$

respectively. Therefore, $d(t)$ is bounded, that is, $|d(t)| \leq d_m := \sup_{t\geq 0}|d(t)|$.

Fig. 2 shows the linear representation of the nonlinear hysteresis operator $\mathcal{H}(\cdot)$ by (3) with the bounded unknown disturbance $d(t)$. Note that for the Duhem model,

$$K(s) = \alpha$$

for the linear system $\mathcal{L}(K, P, d)$ shown in Fig. 1. It is also noted that, although we describe the decomposition process by using the Duhem model, the same conclusion can be always obtained for a general hysteresis relationship.
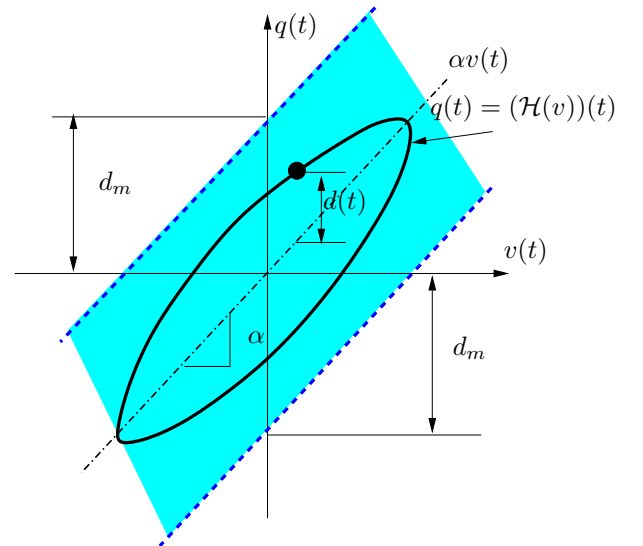

Fig. 2. Schematic of the linear representation for the hysteresis operator $q(t) = (\mathcal{H}(v))(t) = \alpha v(t) + d(t)$.

With the above decomposition, we are now ready to apply the DOB scheme for the nonlinear hysteretic dynamic system (1).

B. DOB-based hysteresis compensation

Fig. 3 shows the block diagram of the DOB-based hysteresis compensation mechanism [8]. Here, $C(s)$ denotes the controller for the plant $\mathcal{L}(K, P, d)$ and $\eta(t)$ denotes the measurement noise. $K_n(s)$ and $P_n(s)$ denote the nominal transfer functions for $K(s)$ and $P(s)$, respectively. It is straightforward to calculate that the estimated disturbance $\tilde{d}(t)$ will be close to real $d(t)$ if the measurement noise $\eta(t)$ is negligible and the nominal plants $K_n(s)$ and $P_n(s)$ are close to $K(s)$ and $P(s)$, respectively.
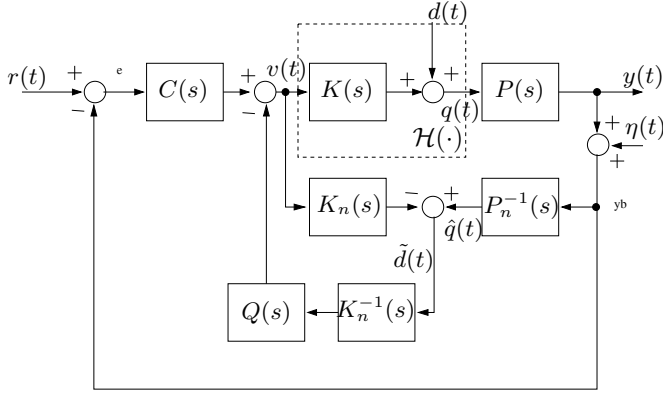

Fig. 3. Schematic of the disturbance observer-based control design.

The filter $Q(s)$ is used to make $Q(s)K_n^{-1}(s)P_n^{-1}(s)$ realizable since $K_n^{-1}(s)$ and $P_n^{-1}(s)$ are typically non-casual. The relative degree of $Q(s)$ must be greater or equal than that of the nominal plant $K_n(s)P_n(s)$ [12]. Moreover, all unstable zeros of $K_n(s)P_n(s)$ must be zeros of $Q(s)$ [13]. Typically, $Q(s)$ can be chosen as [12]

$$Q(s) = \frac{\sum_{k=1}^{N-r} \beta_k(\tau s)^k + 1}{\sum_{k=1}^{N} \beta_k(\tau s)^k + 1},$$

where r is the relative degree of Q.

The stability of the DOB-based control design has been recently presented in [14], [15]. If we design the outer-loop controller $C(s)$ to stabilize the nominal plant $P_n(s)$, real plant $P(s)$ is of minimal phase, and some moderate requirements on the filter design $Q(s)$, the DOB-based hysteresis compensation and control are stable even under the existence of plant uncertainties. We omit the proof here due to the page limit.

III. MODELING OF A PMN-PT PIEZOELECTRIC ACTUATOR

In this section, we first briefly describe the used piezoelectric cantilever actuator and then present a dynamic model of the actuator. More detailed modeling discussion can be found in [16], [17].

The actuator is made of a single crystal relaxor ferroelectric material, PMN-PT. An interdigitated electrode (IDE) design is employed for better actuation performance. To reduce the stress concentration at the support and therefore increase the reliability of the actuator for cyclic loading, we use polydimethylsiloxane (PDMS) to form a coating layer on the PMN-PT cantilever. A proof mass at the cantilever tip is also formed by PDMS to emulate any attached end-effector of micro-/nano-manipulation. Fig. 4 shows the PMN-PT/PDMS cantilever prototype (8 mm × 8 mm × 1 mm) that is attached to a PCB board.

Relative to the PMN-PT layer, the PDMS layer is thin and soft. Therefore, the dual layer structure is considered as a single-layer; see Fig. 5. We denote the size of the PMN-PT cantilever beam as l (length) × b (width) × h (height). Let M_p denote the mass of the proof mass and m the mass density per unit length of the PMN-PT beam.
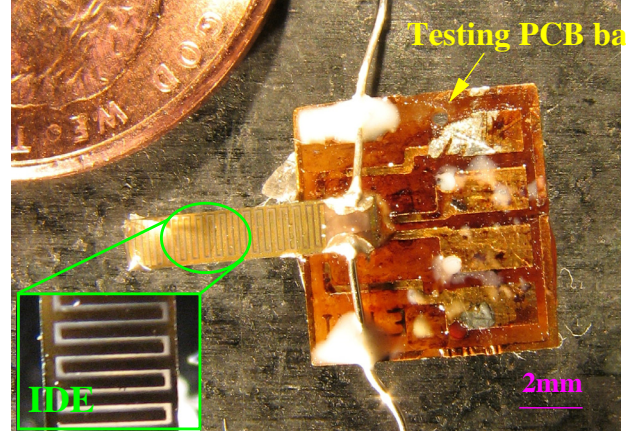

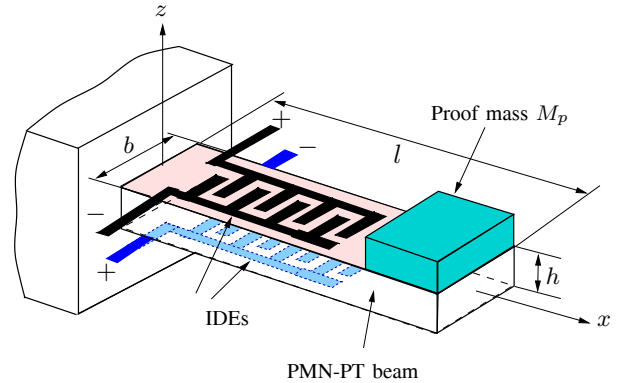Fig. 4. A PMN-PT/PDMS cantilever actuator.

Fig. 5. Schematic of the PMN-PT actuator with IDEs.

Let EI denote the flexural rigidity of the PMN-PT cantilever. We set up the coordinate system such that the x-axis is along the axial direction and the deflection is along the z-axis direction (Fig. 5). The vertical deflection of the beam is denoted by $w(x,t)$ at location x and time t. The kinetic and potential energy of the system are, respectively, as

$$T = \frac{1}{2}\int_0^l m\dot{w}(x,t)^2 dx + \frac{1}{2}M_p\dot{w}(l,t)^2,$$

$$V = \frac{1}{2}\int_0^l EI\left(w''\right)^2 dx,$$

where $\dot{w}(x,t) := \frac{\partial w(x,t)}{\partial t}$ and $w''(x,t) := \frac{\partial^2 w(x,t)}{\partial x^2}$. Let c denote the viscous damping coefficient for the beam. The

virtual work is

$$\delta W_c = \int_0^l \left(-c\dot{w}(x,t) + M_n''(x,t) \right) \delta w dx,$$

where δw is the virtual displacement and $M_n(x,t)$ is the bending moment due to the electric field by the input charge $q_B(t)$ (bottom electrode) and $q_T(t)$ (top electrode).

Let $v_T(t)$ and $v_B(t)$ denote the applied voltages on the top and bottom electrodes, respectively. Let $v_d(t) := v_T(t) - v_B(t)$ and $q_d(t) := q_T(t) - q_B(t)$. We describe the relationship between the voltage $v_d(t)$ and charge $q_d(t)$ as a hysteresis relationship [10], that is, $q_d = (\mathcal{H}(v_d))(t)$. Moreover, $M_n(x,t)$ is approximated [16] as $M_n(x,t) = K_e q_d(t)$, where $K_e := -\frac{Ebd_{33}C_Eh^2}{12h_F}$, C_E is the capacitance of the IDE, h_F is the inter-electrode distance, and d_{33} is the piezoelectric coefficient. We assume that the electrode is fabricated on the beam between location $x_s \geq 0$ and $x_e \leq l$. Therefore, the spatial derivative $M_n''(x,t)$ can be represented as

$$M_n''(x,t) = K_a q_d(t), \tag{6}$$

where $K_a := K_e \left[\delta'(x - x_s) - \delta'(x - x_e) \right]$, and $\delta'(\cdot)$, the spatial derivative of the Dirac delta function, represents the unit dipole function [18].

Using the extended Hamilton's principles, we obtain the equations of motion and boundary conditions

$$M_p \frac{\partial^2 w(l,t)}{\partial t^2} + m \frac{\partial^2 w}{\partial t^2} + c \frac{\partial w}{\partial t} + EI \frac{\partial^4 w}{\partial x^4} = M_n''(x,t), \tag{7a}$$

$$w(0,t) = w'(0,t) = w''(l,t) = 0. \tag{7b}$$

We define $\xi := \frac{x}{l}$, $\gamma_m := \frac{M_p}{ml}$, and $\lambda^4 := \frac{ml^4\omega^2}{EI_{eq}}$ as the dimensionless length of the beam, mass ratio of the proof mass and the beam, and the natural frequency parameters of the beam-mass system, respectively. The characteristic equation of the dynamic systems given in Eq. (7) is then obtained as

$$1 + \cos\lambda\cosh\lambda + \lambda\gamma_m \left(\cos\lambda\sinh\lambda - \sin\lambda\cosh\lambda \right) = 0. \tag{8}$$

The natural frequency decreases as γ_m increases (or as the tip mass increases) [17].

To obtain a generalized single-degree-of-freedom (SDOF) equation of motion, we use the generalized SDOF approximation described in [19]. By variable separation, we write $w(x,t) = \phi(x)p(t)$, where $\phi(x)$ is the modal shape and $p(t)$ is the generalized coordinate for the SDOF system. We consider the following mode shape $\phi(x)$ for the beam-mass systems

$$\phi(x) = \sin(\lambda\xi) - \sinh(\lambda\xi) - B \left[\cos(\lambda\xi) - \cosh(\lambda\xi) \right],$$

where $B(\xi) = \frac{\sin(\lambda\xi)+\sinh(\lambda\xi)}{\cos(\lambda\xi)+\cosh(\lambda\xi)}$. Using expansions for hyperbolic functions, $\phi(x)$ can be approximated as

$$\phi(x) = A\xi^2 - C\xi^3, \tag{9}$$

where $A = B(1)\lambda^2 = \frac{\sin\lambda+\sinh\lambda}{\cos\lambda+\cosh\lambda}\lambda^2$, $C = \frac{1}{3}\lambda^3$.

Using the generalized SDOF system method, the equation of motion for the beam-mass systems in terms of $p(t)$ is obtained as

$$m_e\ddot{p}(t) + c_e\dot{p}(t) + k_ep(t) = f_eq_d(t), \tag{10}$$

where m_e, c_e, k_e, and f_e are generalized mass, damping, stiffness, and force coefficients, respectively [17], [19]. Let $w_p(t) := w(l,t) = \phi(l)p(t)$ denote the measurable tip displacement. From Eqs. (10) and the relationship $w_p(t) = (A - C)p(t)$, we find the transfer function between the excitation charge $q_d(t)$ and the tip displacement $w_p(t)$ as

$$P(s) := \frac{W_p(s)}{Q_d(s)} = \frac{(A - C)f_e}{m_es^2 + c_es + k_e} = \frac{A_v\omega_n^2}{s^2 + 2\zeta\omega_ns + \omega_n^2}, \tag{11}$$

where $\omega_n^2 = \frac{k_e}{m_e}$, $2\zeta\omega_n = \frac{c_e}{m_e}$, and $A_v = \frac{(A-C)f_e}{k_e}$.

IV. EXPERIMENTS

A. Experimental setup

A PMN-PT cantilever actuator prototype (shown in Fig. 4) was fabricated with a dimension of 7.4 mm × 2 mm ×110 μ m. To test the cantilever actuator, we setup a testbed as shown in Fig. 6. The cantilever actuator is mounted on a fixed base. A high-precision fiber optic displacement sensor system (model D11, Philtec Inc.) is used to measure the tip displacement of the cantilever. The cantilever actuator is driven by an amplifier (model 790A, PCB Piezotronics Inc.). A real-time control system (model ACE1104, dSPACE Inc.) is used to control the motion of the actuator and also to collect the displacement data.
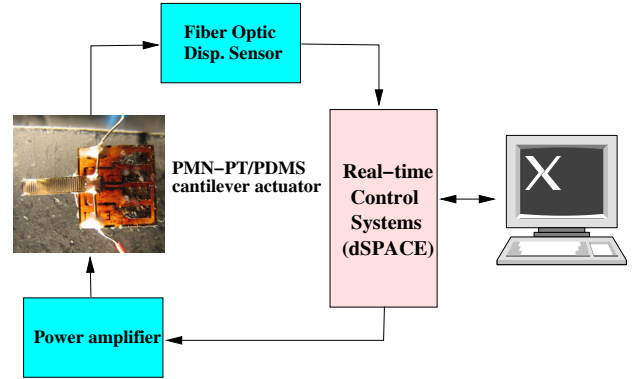

Fig. 6. A schematic of the actuator testing systems.

B. Experimental results

In all experiments, we only excite the electrode on the top surface. The bottom electrode is connected to ground. Therefore, input $v_d(t) = v_T(t)$ and $q_d(t) = q_T(t)$.

We first estimate the model parameters: natural frequency ω_n and damping ratio ζ, in $P(s)$. We excite the cantilever actuator by an impulse voltage and record the resulting response. Fig. 7 shows the frequency plots of the cantilever actuator due to an impulse response and the identified system. Furthermore, we split the original time-domain signal

into segments by their frequency components and then attain the evolution of the modal amplitudes over time. A least-square method is then used to estimate the decay rate and thus obtain an estimate of damping ratio ζ. From the system spectral analysis, we estimate the first natural frequency and damping ratio to be

$$\omega_n = 1547 \text{ Hz}, \quad \zeta = 0.00876.$$

We cannot measure the charge signal $q(t)$ in experiments. Also, from an input/output viewpoint, the actuator system has two sets of dc-gain parameters, α in the hysteresis operator (3) and A_v in the plant (11). Therefore, we choose $A_v = 1$ C/V and let the system dc-gain be determined by the value of α. Fig. 8(a) and 8(c) show the actuator response under a sinusoidal input with a frequency of 10 Hz and 100 Hz, respectively. From the results, the hysteresis nonlinearity in actuator response is apparently independent of input frequency. We can then estimate the value of α by using the responses under various input frequencies, and the following estimate is obtained.

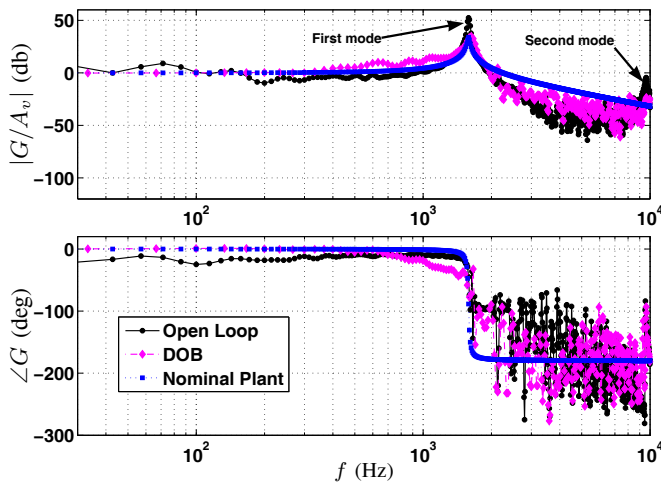$$K(s) = K_n(s) = \alpha = 76.4 \text{ nm/C}.$$

Fig. 7. Bode plot of the cantilever impulse input and feedback responses under DOB.

To demonstrate the effectiveness of the DOB-based hysteresis compensation, two experimental examples are shown in Fig. 8(b) and 8(d). In these figures, we can see the tip displacement versus input voltage relationship under a compensation of the DOB design. Since the plant dynamics $P(s)$ is stable and minimum-phase, we choose a second-order Butterworth filter for $Q(s)$, namely,

$$Q(s) = \frac{\omega_c^2}{s^2 + \sqrt{2}\omega_c s + \omega_c^2},$$

where ω_c is the cutoff frequency of the filter. We have found that for stability, the cutoff frequency ω_c needs to be below approximately 500 Hz, and therefore we choose $\omega_c = 500$ Hz in our experiments. Although we demonstrate, here, the effectiveness of the proposed hysteresis compensation under only two input frequencies, our other testing results have

demonstrated a successful compensation up to 200 Hz input frequency.

A PID controller $C(s)$ is used to track the reference signal $r(t)$ in the DOB-based control system design shown in Fig. 3. The gains for the PID controller $C(s)$ are tuned as

$$K_p = 10^{-4}, \ K_i = 125, \ K_d = 10^{-10}$$

for achieving the best performance under a step input $r(t)$. To compare the tracking performance with and without the DOB compensation, we keep these gains unchanged in both experiments. Fig. 9 shows the comparison result of a step response. We observe that without hysteresis compensation, the response has a slower response time (around 50 ms) while using the DOB-based hysteresis compensator, we are able to obtain a much faster response with almost no delay.

V. CONCLUSION

In this paper, we demonstrated a novel hysteresis compensation method with applications to piezoelectric actuators. The compensation mechanism treats the hysteresis nonlinearity as an unknown disturbance added to a linear system. As a result, the proposed hysteresis compensation method does not rely on any mathematical model of hysteresis. Simplicity in implementation and robustness of performance are the main advantages of the DOB-based hysteresis compensation approach. We have demonstrated the effectiveness and efficiency of the method as applied it to a PMN-PT cantilever piezoelectric actuator within a dynamic bandwidth of 100 Hz.

Improving dynamic performance of the proposed hysteresis compensator is an ongoing research. We are also interested in enhancing the DOB-based design for high-bandwidth hysteresis compensation that can be applied for micro-/nano-manipulation systems.

REFERENCES

[1] T. Fukuda, F. Arai, and L. Dong, "Assembly of nanodevices with carbon nanotubes through nanorobotic manipulations," *Proc. IEEE*, vol. 91, no. 11, pp. 1803–1818, 2003.
[2] N. Xi and W. Li, "Recent development in nanoscale manipulation and assembly," *IEEE Trans. Automat. Sci. Eng.*, vol. 3, no. 3, pp. 194–198, 2006.
[3] S. Devasia, E. Eleftheriou, and S. Moheimani, "A survey of control issues in nanopositioning," *IEEE Trans. Contr. Syst. Technol.*, vol. 15, no. 5, pp. 802–823, 2007.
[4] X. Tan and R. Iyer, "Modeling and control of hysteresis," *IEEE Control Syst. Mag.*, vol. 29, no. 1, pp. 26–29, 2009.
[5] H. Janocha, D. Pesotski, and K. Kuhnen, "FPGA-based compensator of hysteretic actuator nonlinearities for highly dynamic applications," *IEEE/ASME Trans. Mechatron.*, vol. 13, no. 1, pp. 112–116, 2008.
[6] J. Macki, P. Nistri, and P. Zecca, "Mathematical models for hysteresis," *SIAM Rev.*, vol. 35, no. 1, pp. 94–123, 1993.
[7] A. Visintin, "Mathematical models of hysteresis," in *The Science of Hysteresis*, G. Bertotti and I. Mayergoyz, Eds. London, UK: The Academic Press, 2006, pp. 1–123.
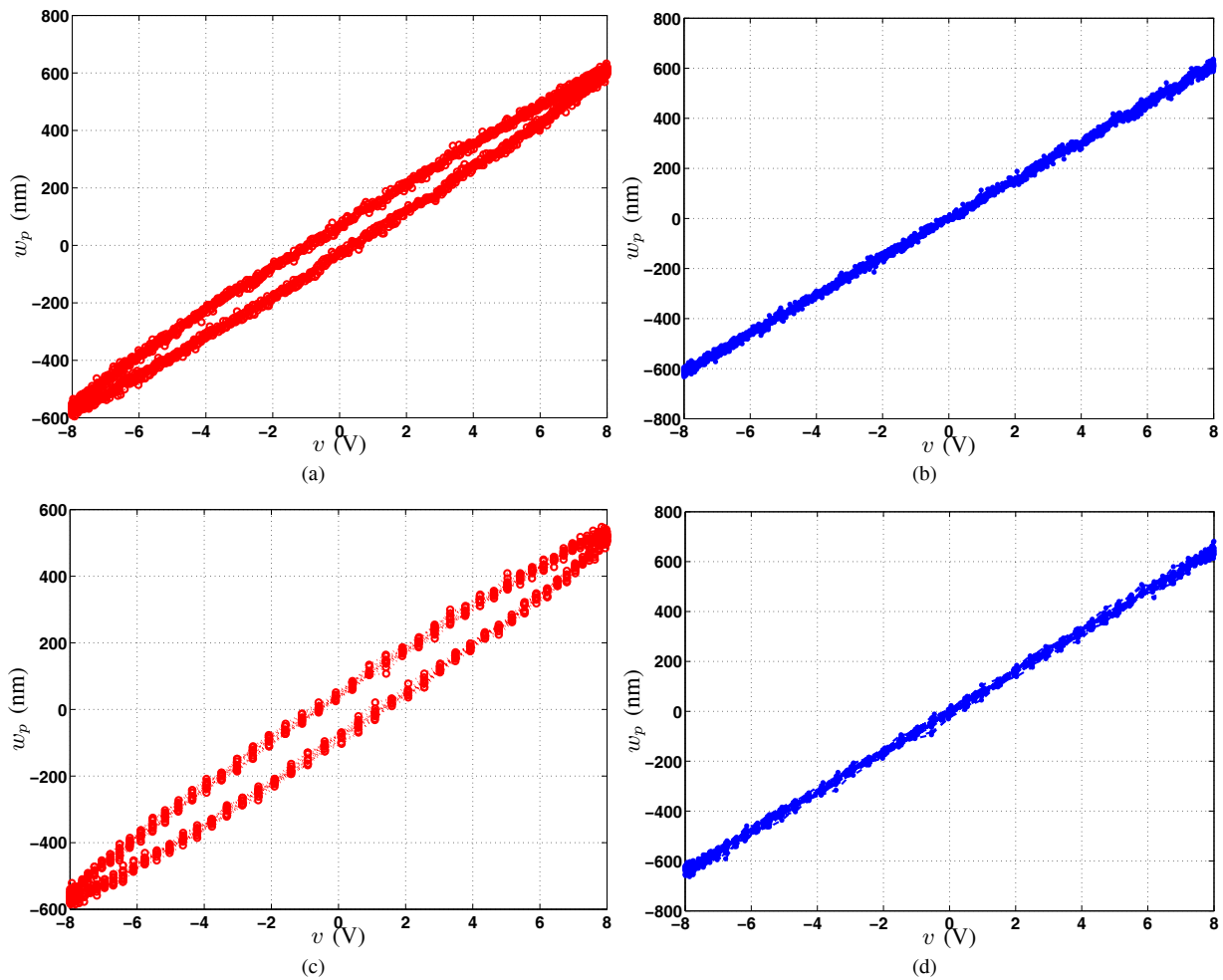
Fig. 8. The tip displacement versus the input voltage. (a) Without DOB under a 10 Hz excitation. (b) With DOB compensation under a 10 Hz excitation. (c) Without DOB under a 100 Hz excitation. (d) With DOB compensation under a 100 Hz excitation.

[8] S. Shahruz, "Performance enhancement of a class of nonlinear systems by disturbance observers," *IEEE/ASME Trans. Mechatron.*, vol. 5, no. 3, pp. 319–323, 2000.

[9] F. Goforth and Z. Gao, "An active disturbance rejection control solution for hysteresis compensation," in *Proc. Amer. Control Conf.*, Seattle, WA, 2008, pp. 2202–2208.

[10] H. Adriaens, W. de Koning, and R. Banning, "Modeling piezoelectric actuators," *IEEE/ASME Trans. Mechatron.*, vol. 5, no. 4, pp. 331–341, 2000.

[11] C.-Y. Su, Y. Stepanenko, J. Svoboda, and T. Leung, "Robust adpative control of a class of nonlinear systems with unknown backlash-like hysteresis," *IEEE Trans. Automat. Contr.*, vol. 45, no. 12, pp. 2427–2432, 2000.

[12] T. Umeno and Y. Hori, "Robust speed control of DC servomotors using modern two-degree-of-freedom controller design," *IEEE Trans. Ind. Electron.*, vol. 38, no. 5, pp. 363–368, 1991.

[13] A. Tesfaye, H. Lee, and M. Tomizuka, "A sensitivity optimization approach to design of a disturbance observer in digital motion control systems," *IEEE/ASME Trans. Mechatron.*, vol. 5, no. 1, pp. 32–38, 2000.

[14] E. Schrijver and J. van Dijk, "Disturbance observers for rigid mechanical system: equivalence, stability, and design," *ASME J. Dyn. Syst., Meas., Control*, vol. 124, no. 4, pp. 539–548, 2002.

[15] H. Shim and N. Jo, "An almost necessary and sufficient condition for robust stability of closed-loop systems with disturbance observer," *Automatica*, vol. 45, pp. 296–299, 2009.

[16] J. Yi, S. Chang, K. Moon, and Y. Shi, "Dynamic modeling of an L-shape PMN-PT piezo-based manipulator," in *Proc. Amer. Control Conf.*, Seattle, WA, 2008, pp. 3755–3760.

[17] A. Mathers, K. Moon, and J. Yi, "A vibration-based PMN-PT/PDMS energy harvester," *IEEE Sensors J.*, in press, 2009.

[18] H.R. Pota and T.E. Alberts, "Multivariable transfer functions for a slewing piezoelectric laminate beam," *ASME J. Dyn. Syst., Meas., Control*, vol. 117, no. 3, pp. 352–359, 1995.

[19] S. Shahruz, "Design of mechanical band-pass filters for energy scavenging," *J. Sound Vib.*, vol. 292, no. 3-5, pp. 987–998, 2006.
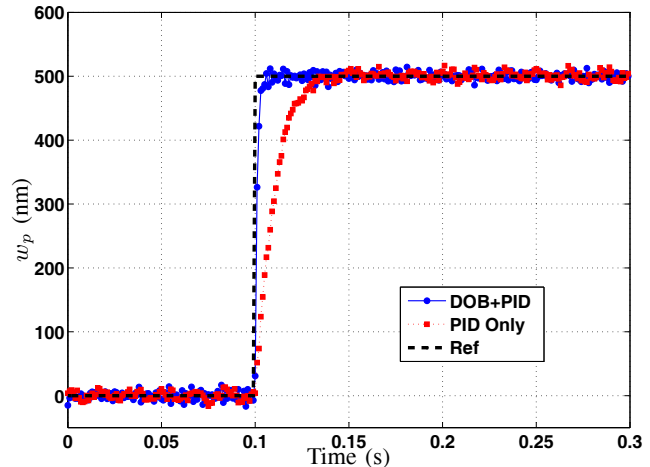
Fig. 9. Comparison results of the step responses with and without the DOB hysteresis compensation.